machines

MDPI

Article

On the "Zero of Potential of the Electric Field Produced by the Heart Beat". A Machine Capable of Estimating this Underlying Persistent Error in Electrocardiography

Gaetano D. Gargiulo [1,2,*], Paolo Bifulco [2], Mario Cesarelli [2], Alistair L. McEwan [3], Hossein Moeinzadeh [1], Aiden O'Loughlin [4], Ibrahim M. Shugman [5], Jonathan C. Tapson [1] and Aravinda Thiagalingam [6]

1 The MARCS Institute, Western Sydney University, Milperra NSW 2214, Australia; h.moeinzadeh@westernsydney.edu.au (H.M.); j.tapson@westernsydney.edu.au (J.C.T.)
2 Department of Electrical Engineering and Information Technology (DIETI), "Federico II" The University of Naples, Naples 80100, Italy; pabifulc@unina.it (P.B.); cesarell@unina.it (M.C.)
3 School of EIE, University of Sydney, Sydney NSW 2006, Australia; alistair.mcewan@sydney.edu.au
4 School of Medicine, Western Sydney University, Campbelltown NSW 2650, Australia; aiden.oloughlin@gmail.com
5 Cardiology Department, Campbelltown Hospital, Campbelltown NSW 2650, Australia; shugmano@hotmail.com
6 School of Medicine, The University of Sydney, Sydney NSW 2006, Australia; aravinda.thiagalingam@sydney.edu.au
* Correspondence: g.gargiulo@westernsydney.edu.au; Tel.: +61-2-4736-0920

Academic Editor: Dan Zhang
Received: 21 July 2016; Accepted: 30 September 2016; Published: 15 October 2016

Abstract: Modern electrocardiography (ECG) uses a constructed reference potential for the majority of leads. This reference potential, named after its inventor as the Wilson central terminal, is assumed to have negligible value and to be stationary during the cardiac cycle. However, the problem of its variability during the cardiac cycle has been known almost since the inception of 12-lead electrocardiography. Due to the cumbersomeness of the measurement system required to fully appreciate these variations, this topic has received scant research attention during the last 60 years. Taking advantage of modern electronic amplifiers' capability to detect small voltages, drawing only femtoamperes from physiological equivalent signal sources and of the right-leg connection availability, we developed a complete electrocardiography device that, aside from the eight independent signals of the standard 12-lead ECG, allows direct recording of the Wilson central terminal components. In this paper, we present details of the circuit together with its initial clinical evaluation. For this trial, we recorded data from 44 volunteer patients at Campbelltown Hospital (Campbelltown, Australia) and we found that the Wilson central terminal amplitude, as foreseen by Frank and others in the 1950s, is not negligible, its amplitude in relation to the lead II is, on average, 51.2%, and thus it may be clinically relevant.

Keywords: electrocardiography; Wilson Central Terminal; potential reference

1. Introduction

The majority of modern-day clinicians and researchers appear to have forgotten that at the base of modern electrocardiography (ECG) is a largely simplifying assumption, that reduces the extremely complex electrical activity of the heart to a single equivalent electrical dipole rotating in the chest around a fixed point. This simplifying assumption, formulated in the 1930s by Wilson [1], allowed

assessment of cardiac electrical activity in the whole body space rather than in its two-dimensional (2-D) projection over the limbs, as originally outlined by W. Einthoven in 1906 [1]. In other words, Wilson devised a virtual stationary fixed point (which was named after him: Wilson central terminal or simply WCT) as a current average of Einthoven's limb electrodes [1].

The assumption of a single dipole rotating around Wilson's virtual fixed point was soon recognized to be the source of potential errors for ECG. In 1954, Frank, in his famous dissertation "General Theory of Heart-Vector Projection" [2] warned clinicians about the use of this oversimplifying assumption. Empirical confirmation of Frank's hypotheses about the amplitude and variability of the WCT came almost simultaneously when measurements of WCT (requiring the human body to be encased in a metal structure totally submerged in water for the duration of the recording), showed that Wilson's central point is non-stationary during the cardiac cycle and has a large amplitude (up to 40% of Einthoven's ECG signal amplitudes). Details of these results were published by both H.C. Burger and R. Bayley et al. [3,4]. However, until now, without a valid alternative, this largely simplified hypothesis still lies at the base of modern clinical practice.

In the late 1950s, the electronic amplifier substituted the original string galvanometer, leading to the ECG gaining in popularity, reducing its cumbersomeness, and allowing simultaneous observation of more than one lead. However, electronic amplifiers required the addition of a further limb to the ECG measurement that original inventors of the system had not taken into account: the "right leg." Remembering that electronic amplifiers, by construction and design, are better equipped to measure voltages rather than currents [5–7], and also bearing in mind that an additional reference terminal may be required for common mode signal rejection reasons, particularly at power-line frequencies [7–10], it was a natural choice for engineers to connect this additional terminal to the right leg [8,9]. The right leg was traditionally excluded from the original Einthoven/Wilson ECG model because the string galvanometer measures directly the current circulating into the surrounding tissues as a consequence of the shift in the electromagnetic field impressed by the heart's activation. Therefore, the original ECG electrical model is arranged as a closed circuit (Einthoven's triangle) and each of its branches includes the heart in the current pathway. As can be inferred from the original model, there is no evident current pathway between the heart and the legs (see Figure 1) [1,11–15].

Taking advantage of the right-leg connection and of the negligible load upon equivalent physiological signal sources offered by modern voltage amplifiers (in the order of femtoamperes [10–15]), we developed a full 15-lead ECG device that, aside from the standard 12-lead signals, can record the independent voltages of the right arm, left arm and left leg. These additional independent voltages (directly referred to the right leg) can be used to:

1) Measure the WCT amplitude without the need to encase the patient into a metal structure submerged in water.
2) Correlate the amplitude of the WCT to the cardinal limb leads.

In this paper, we detail the hardware used together with the results of our clinical evaluation. For this clinical evaluation, we recorded data from 44 patients at Campbelltown Hospital (NSW) and we measured the amplitude of the WCT and correlated it with the amplitude of lead II. We found that the amplitude of the WCT could exceed the amplitude of lead II and on average across our entire population, WCT amplitude is 51.2% of lead II. All the patients volunteered for this study and gave written consent (this study was approved on 23 September 2015 with the protocol number HREC/15/LPOOL/302).

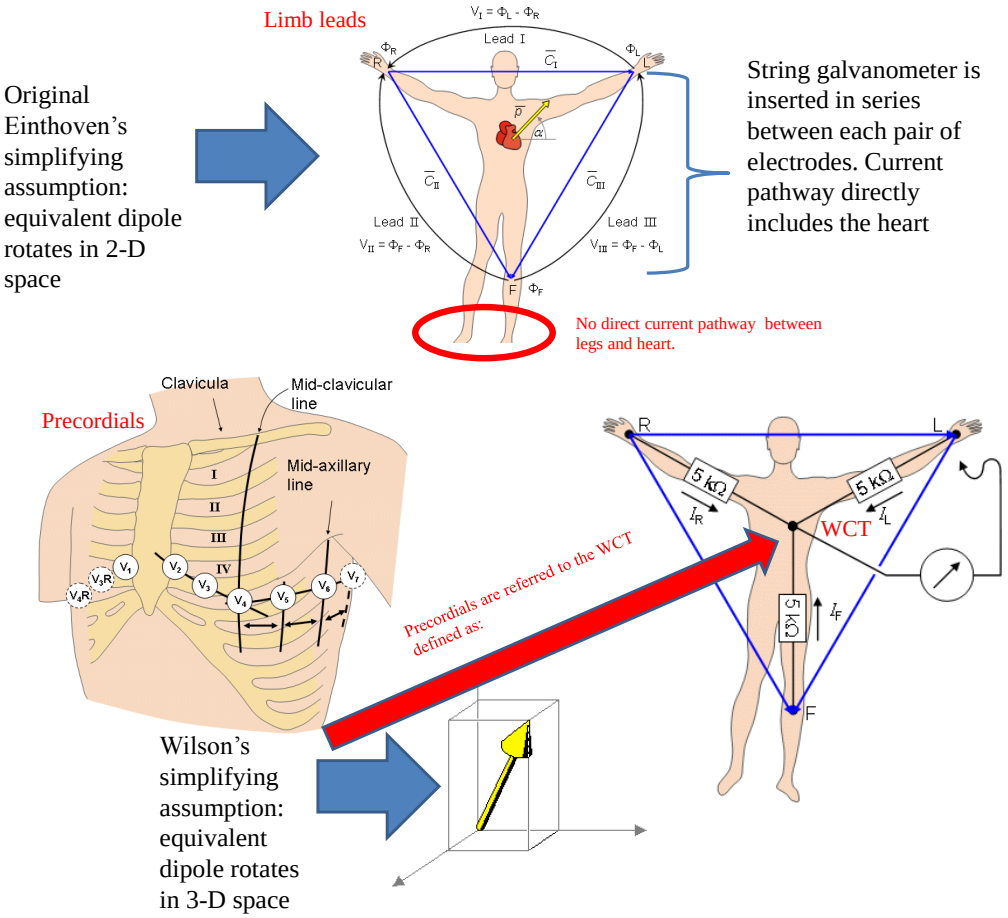

Figure 1. ECG conduction model evolution: Original Einthoven model (top), which included only the three limbs that form a triangular circuit around the heart, whereas the heart is included in each branch current pathway; Wilson's precordial leads (bottom) with WCT definition as current return formed as the center of Einthoven's triangle (bottom right). Modified from [1].

2. Methods

We designed our hardware around the instrumentation amplifier INA116 [16], manufactured by Texas Instruments, Dallas, TX, USA (Burr-Brown series). According to the chip specifications, its bias current (i.e., the load to the physiological signal source) is typically only 5 fA. This extraordinarily small value is achieved by the combination of an extremely high input impedance with a relatively small parasitic capacitance and embedded active guard ring buffer (see technical documentation [16] for precise details). In order to preserve the mentioned characteristics, the printed circuit board is designed to take advantage of the embedded active guard ring amplifier on a Teflon substrate. Although the guard ring amplifier's primary job is to reduce the noise pick-up at cable and board connections, because this offers a replica of the input signal, we also use it to measure the raw voltage of the WCT components [17–20].

To ensure high conductivity of connections between pins and exposed pads on the board, the latter are silver-plated by immersion during manufacturing. To avoid smearing of solder under the chip body and between pins during soldering, the chip body is sealed in position prior to soldering, using a suitable printed circuit board non-conductive epoxy resin. As an additional precaution, the conductivity between electrode connections and chip pins is verified prior to soldering, using a multimeter. Each pin of the INA116 is then manually soldered to the pad using lead-free silver-based paste with a 0.2 mm diameter hot iron tip. To further minimize parasitic capacitance at board level, the guard ring pattern is repeated on each layer of the board and aside from the chips' necessary

connections, no other traces are routed in the area under each INA116. As a last precaution, as recommended in the existing literature, wire connections to the chip are directly soldered to the board on the top layer (no thru-hole connections) [10,21–23]. Finally, the assembled board is coated with conformal coating to protect it from moisture that could contaminate the board due to its use in the hospital environment (frequent cleaning and wiping of the enclosure/cables with disinfectant).

The simplified schematic of the hardware, limited to the four limbs and one of the precordials, is depicted in Figure 2. Protection from electrostatic discharges is achieved by interconnection of a single high-precision low-noise Panasonic surface mount ECG series 100 kΩ resistor. Protection against defibrillation discharges and simultaneous high-impedance biasing of the INA116 electrodes' connections is achieved by parallel connection of low-voltage activation gas discharge tubes; with an arc voltage as low as 15 V [24] they protect the sensitive chip inputs even for voltages that are lower than the embedded overvoltage protection [24]. Discharge tubes also offer the perfect biasing pathway for INA116 due to their nominal resistance >10 GΩ and a negligible parasitic capacitance. To avoid cluttering Figure 2, the gas discharge tubes are not represented.

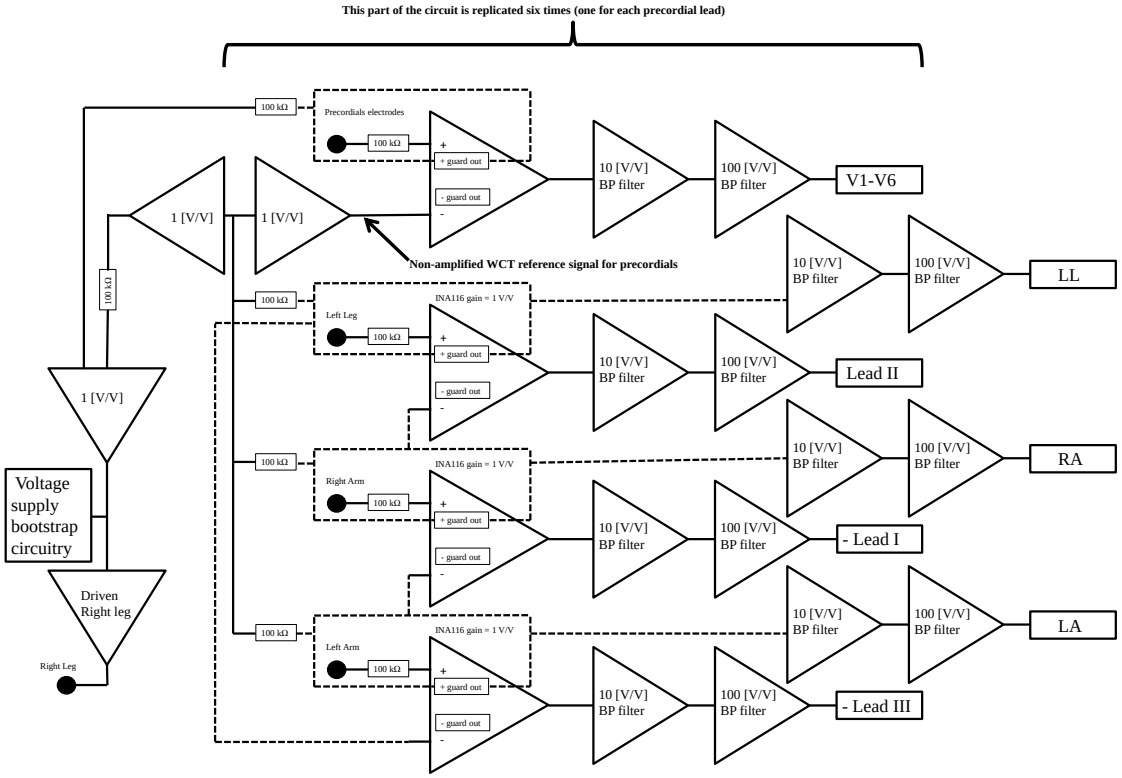

Figure 2. Simplified schematic limited to limbs' connections and one of the precordials.

As mentioned, and as it is possible to infer from the schematic, the guard buffer of the left-leg, left-arm and right-arm electrodes are also used to directly measure the WCT components' voltages. The gain set for the INA116 chips is 1 V/V, achieved by leaving pins 1 and 8 floating (not noted in Figure 2). Necessary gain and band bass filtering is achieved by two AC coupled active non-inverting low-pass filters gaining 10 V/V and 100 V/V, respectively. Each gain cell is designed around the amplifier chip OPA140 [25]. Aside from its very low-noise figure, the OPA140 has been selected because of its high slew rate, immunity from phase inversion and very low current-bias. Owing to these characteristics, we have designed a high-gain non-inverting band-pass filtering gain cell that does not require additional biasing and copes well with the frequent swings between saturation voltages due to ECG artefacts. Aside from the value of some passive components to achieve different gains, the gain cells are identical. The simplified schematic of the gain cell is depicted in Figure 3.

In order to achieve a diagnostic quality ECG, both the high-pass and low-pass corner frequencies of the gain cell are set with capacitors whose value has been selected to be larger than the theoretical values. In this way, even in the worst case scenario of a −10% value due to the capacitor tolerances, the required bandwidth is assured. Frequency content normalization to the diagnostic bandwidth is operated via software after signal acquisition. Components' values are reported in Table 1 for both gain cells. Differences between values of components are highlighted in bold. As an additional precaution, high-precision Murata ceramic capacitors have been used.

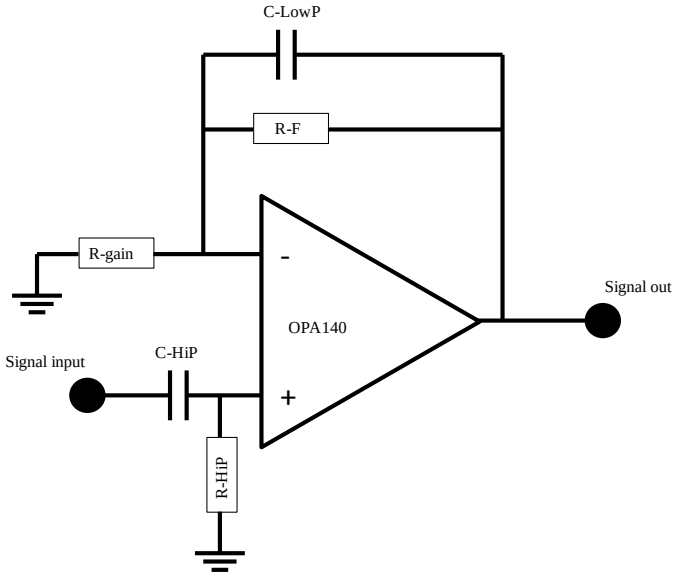

Figure 3. Active band-pass filter gain cell, see Table 1 for components' values.

Table 1. Summary of components' values for the gain cells.

Component	10 V/V Gain Version	100 V/V Gain Version
C-HiP	47 µ	47 µ
R-HiP	100 kΩ	100 kΩ
C-LowP	15 nF	1.5 nF
R-F	100 kΩ	1 MΩ
R-gain	10 kΩ	10 kΩ

As noted in Figure 2, the circuit includes a modified voltage bootstrap circuitry [18,20,26–28] that directly drives the reference voltage of the circuit with a damped version of the average of all the electrodes. This solution proved successful in all of our past circuit implementations [18,20,29], particularly when the right-leg connection is included in the average. However, for this implementation we introduced a driven-right-leg circuitry designed and dimensioned to contain current drive to 20 µA [8,30,31]. The input signal for the driven-right-leg circuitry is the non-amplified average of the measurement electrodes (see Figure 2).

The entire circuit is powered by a dual 9 V power supply formed by two 9 V batteries in series that proved sufficient for a day of recordings in the hospital. Digital conversion and data logging is operated at a 16-bit depth over the range of ±5 V at the sample rate of 800 Hz by the BIOADC [32], powered directly by the USB connection to a host laptop computer (battery-powered). Necessary anti-aliasing low-pass filtering at the Nyquist frequency is embedded in the BIOADC. The entire system is hosted on a standard hospital instrumentation trolley that allows easy transportation of the device around rooms and ambulatories for the recording. More details pertaining to the hardware tests are reported in Appendix A.

Recorded data have been firstly assessed for quality, comparing visually the shapes and amplitude of 12-lead ECG traces recorded by our machine with the one obtained from the resident device used for routine investigation. Data sets, whose amplitude and shapes passed the visual test, have been included in this database (100% inclusion). For this study, we measured the WCT amplitude and reported it as a percentage of lead II in 44 patients who had volunteered for the study. We also report the polarity of the WCT based upon the orientation of the QRS feature present in the signal. Similarly to previous studies [3,4], we noted that with "N" signals, polarity is not clearly positive or negative i.e., the positive deflection amplitude almost matches the negative deflection at the QRS feature. Reported amplitude measurements are averaged across at least five consecutive beats. To compare the WCT's amplitude we selected lead II because, according to the circuit principles applied to the electrocardiography (see Figure 1), lead II is the result of the sum of lead I and lead II. Therefore, lead II should be the largest of the limb leads [1]. Furthermore, lead II is used as a calibration signal from many patient simulators used in standard engineering practice and often represented, at the bottom of the standard clinical ECG diagnostic sheets, longer traces for cardiac rhythm assessment.

3. Results

Bench tests of the assembled prototype show that the gain of each channel is 1023 $\pm$ 5% V/V and the bandwidth contains the diagnostic ECG frequency [1,8]. A custom-made import script takes into account precise measured gains, normalizes the frequency content to 0.05–150 Hz via a 50th order Infinite Impulsive Response (IIR) band-pass filter; and removes power-line noise at 50 Hz and harmonics up to the Nyquist frequency, via a batch of 50th order IIR notch filters each with a quality factor of 35. All filters have been implemented as "non-causal" to avoid introducing phase delays.

As mentioned, only data sets that passed the visual inspection test (see Methods section) have been included in this data set. A total of twelve recordings have been discarded due to the necessity to abort the recording (i.e., patient required transportation to other wards for procedures) or due to the presence of large artifacts or the persistent presence of pacemaker activations on the recorded traces. Of the 44 recordings, 17 patients were female. The average age of the study's patient population is 66.8 years (with a standard deviation of 13.4 years); the majority of the patients have a history of cardiac disease and have been admitted to the hospital from the emergency department because of difficulties in breathing and/or chest pain.

The summary of our measurement results is reported in Table 2 for each patient. Amplitude of the WCT is measured as a relative percentage of lead II. The average WCT amplitude for our data set is 51.2% of lead II with a standard deviation of 27.4%, which is slightly larger than that described in the existing literature [1,8], where relative amplitudes of up to the 40% are reported. However, those studies used a different and cumbersome setup and date back to the 1950s. Nevertheless, to our surprise, for several patients, the amplitude of the WCT is as large as lead II, with several beats in which WCT's amplitude exceeds lead II by up to 20%; in Table 2, all of the cases where the WCT's average amplitude was larger than 99% of lead II, were approximated with 100%. Although positive deflection of WCT seems to be the majority (see Table 2), with only a handful of neutral (noted with N) polarities, it is not possible to find characteristic or uniform shapes of WCT. Based upon our measurements, WCT is highly individual, can have standard ECG characteristics, such as a p-wave and a t-wave, and thus should be included in the ECG signal space used for diagnosing diseases.

An example of the WCT signal with a marked t-wave is visible in Figure 4. As can be seen, a marked t-wave deflection on the WCT trace (bottom panel) is synchronized with the t-wave on lead II (top panel). The WCT trace in Figure 4 is also a good example of a highly variable WCT, which in one single cardiac cycle changes the deflection's polarity at least three times, with an amplitude that reaches 65% of lead II (average).

An example of high-amplitude WCT is depicted in Figure 5. As can be seen, the amplitude of the WCT (positive deflection) has a similar amplitude to the lead II with a broader QRS feature. In Figure 6 we present an example of multimodal WCT: for this patient, on average the WCT has

a positive deflection, and shape alteration is observable during ectopic beats, where the WCT exhibits a broader QRS. Other examples of WCT which mutate from positive deflection to almost neutral and fully negative during ectopic beats are depicted in Figures 7 and 8.

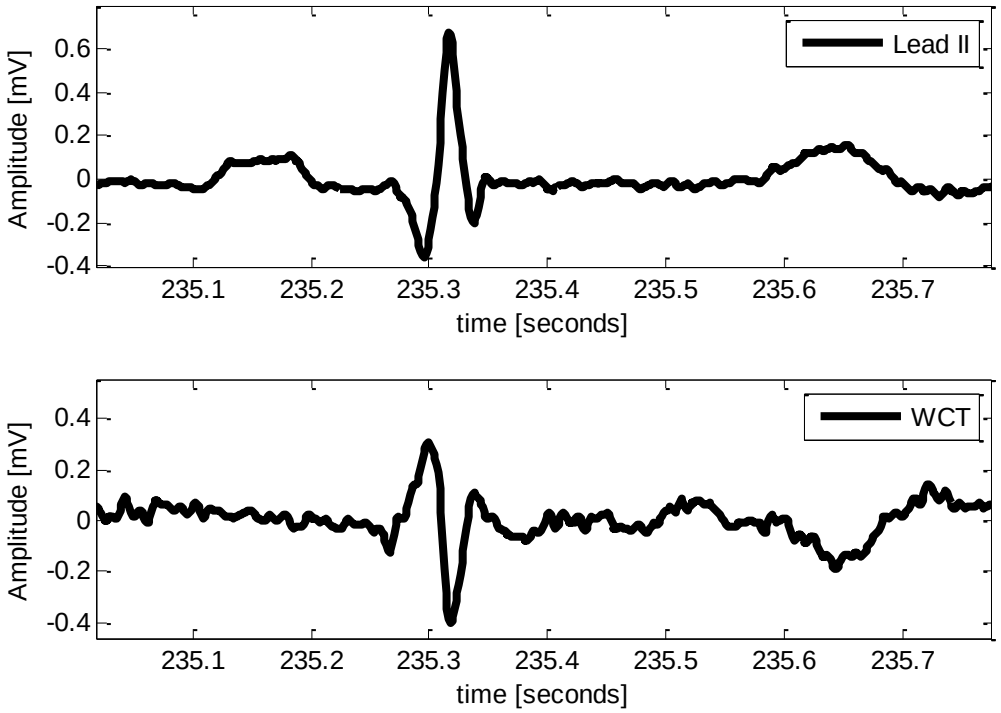

Figure 4. Example of negative deflection WCT. WCT is 65% of lead II amplitude (average); recording is from a 70-year-old female patient admitted with chest pain. WCT for this patient presents a marked t-wave.

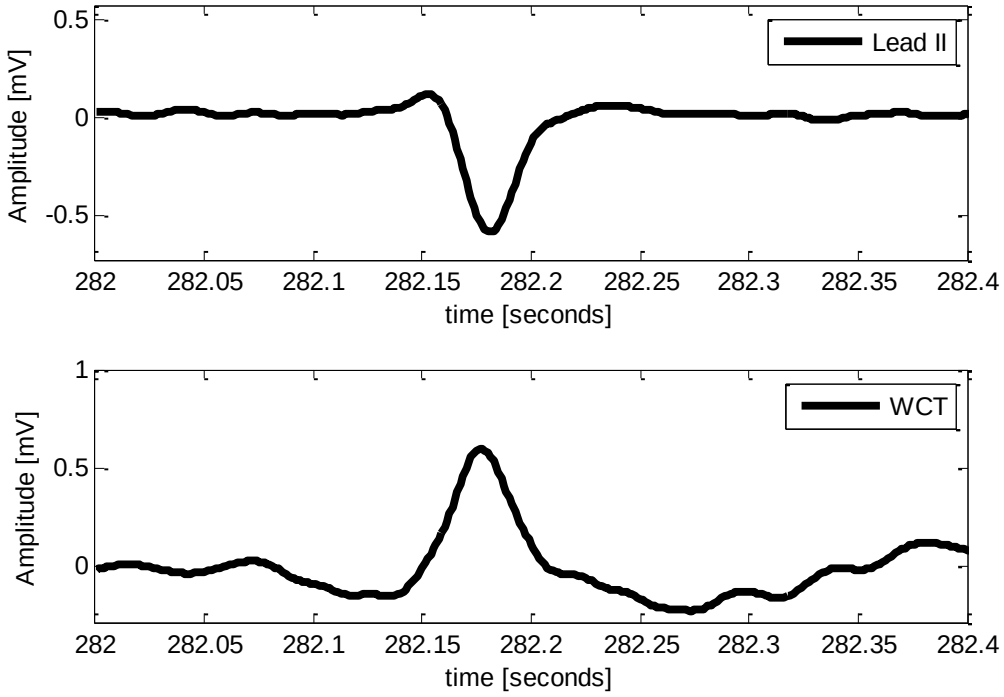

Figure 5. Example of positive deflection WCT. WCT is 100% of lead II amplitude (average); recording is from an 82-year-old female patient admitted from the emergency department (unconfirmed diagnosis).

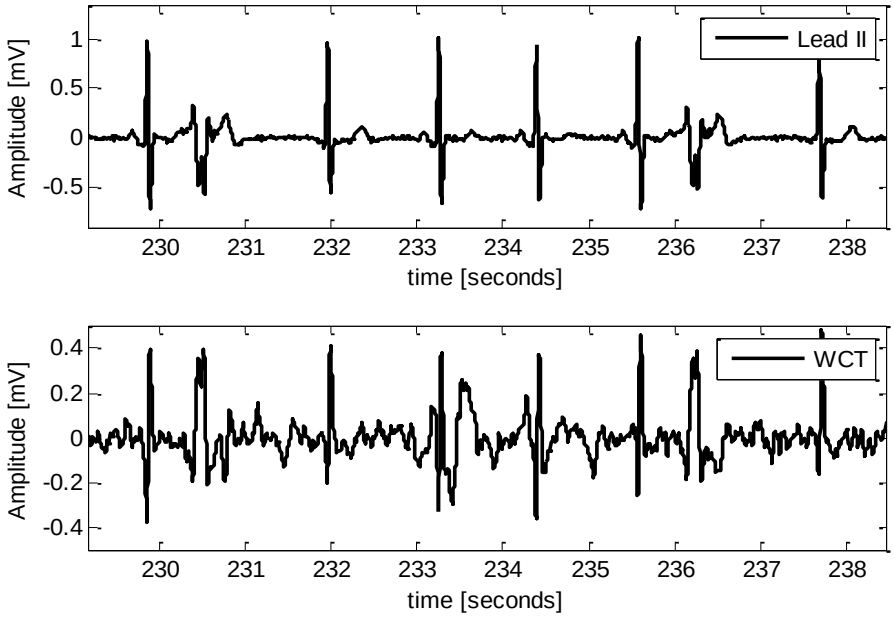

Figure 6. Example of multimodal WCT with severe alteration during ectopic beats (noted with a black arrow). WCT is 45% of lead II amplitude (average); recording is from a 72-year-old female patient admitted from the emergency department with severe chest pain.

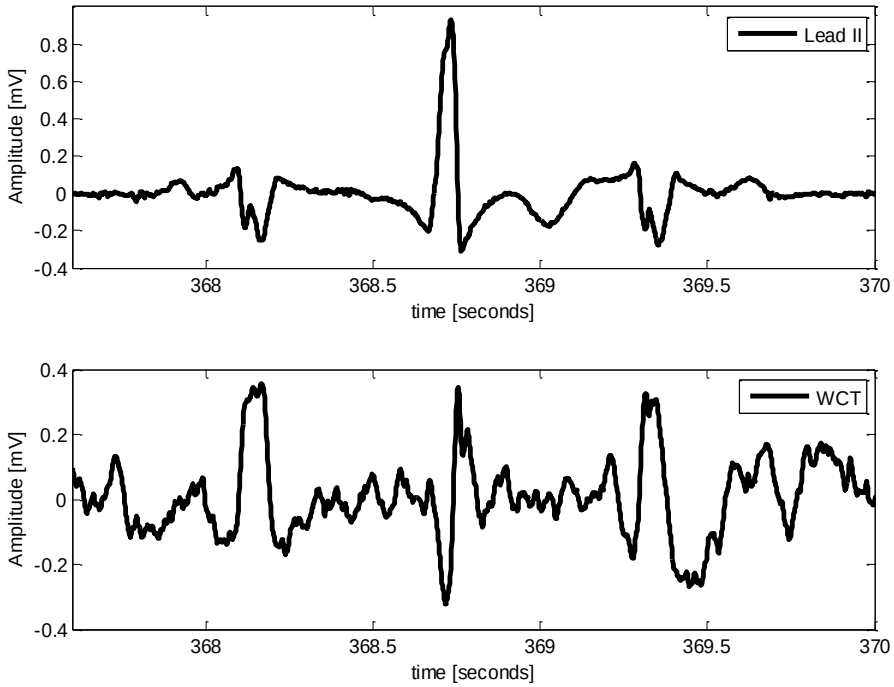

Figure 7. Example of positive WCT that mutates into almost neutral (almost identical value for positive and negative peak) during an ectopic beat (noted by the arrow). WCT amplitude also varies from >100% of lead II amplitude (average) to approximately 50% of lead II during the ectopic beat; recording is from an 85-year-old male patient admitted from the emergency department with severe chest pain and unconfirmed myocardial infarction.

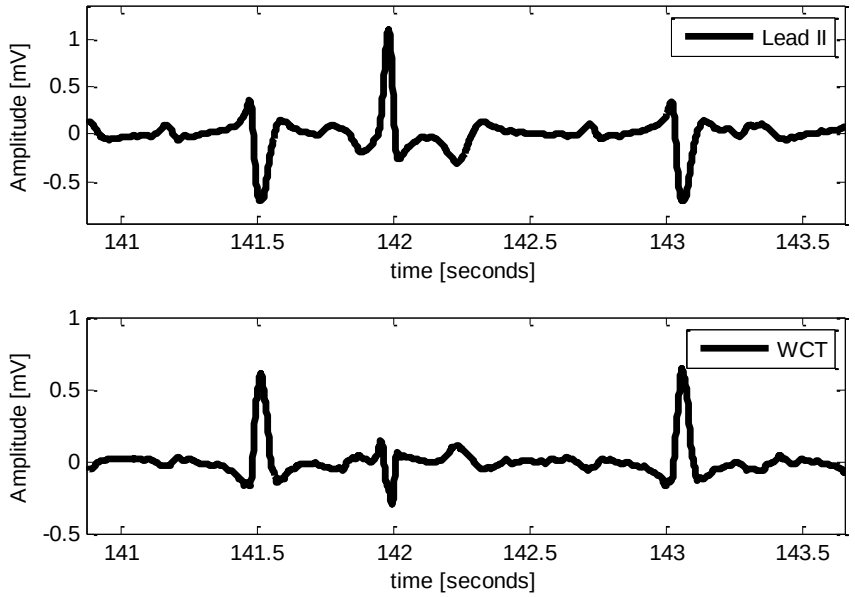

Figure 8. Example of positive WCT that mutates into negative during an ectopic beat (noted by the arrow). WCT amplitude also varies from 65% of lead II amplitude (average) to 33% of lead II during the ectopic beat; recording is from a 79-year-old male patient admitted due to arrhythmia.

In Figure 9, we show an example of WCT that exhibits all of the characteristics of an ECG trace. For this patient, the WCT has a marked p-wave and t-wave that, for some beats, have a larger amplitude than the multimodal QRS complex. This is another example of highly variable WCT, which in this case changes deflection polarity at least five times into a single cardiac cycle. Of note, from Table 2 it is possible to observe that the relative amplitude of the WCT, with respect to lead II, is below 15% for only one patient.

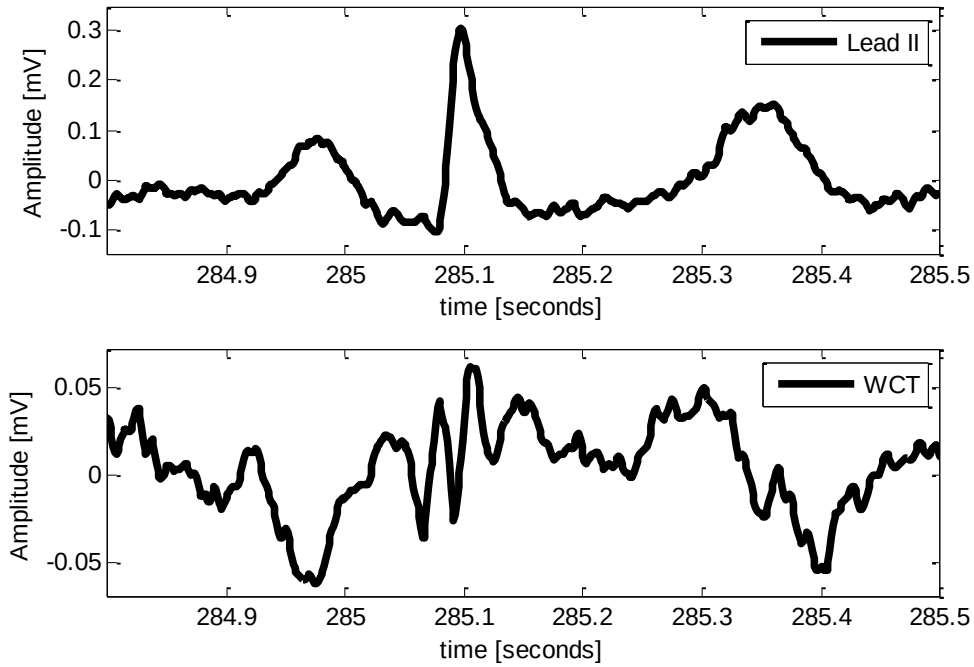

Figure 9. Example of multimodal WCT with evident features in correspondence with "p" and "t" waves. WCT is 23% of lead II amplitude (average); recording is from a 63-year-old female patient admitted from the emergency department with severe chest pain.

Table 2. Summary of measurement results. WCT relative amplitudes are approximated to the nearest integer and capped to 100% for the measurements larger than 99% (see text).

Patient ID	Age (y.o.)	Gender	WCT Amplitude As % of Lead II	WCT Polarity	Figure
P001	63	F	27	+	
P002	51	F	40	+	
P003	65	F	35	−	
P004	63	F	30	+	
P005	88	F	90	+	
P006	52	F	90	+	
P007	70	F	59	+	
P008	55	F	44	+	
P009	82	F	12	−	
P010	71	F	23	+	
P011	69	F	19	+	
P012	89	F	25	−	
P013	63	F	23	+	Figure 9
P014	70	F	41	N	
P015	72	F	45	+	Figure 6
P016	70	F	65	−	Figure 4
P017	82	F	100	+	Figure 5
P018	59	M	100	−	
P019	68	M	33	−	
P020	79	M	65	+	Figure 8
P021	55	M	50	+	
P022	71	M	40	N	
P023	52	M	60	+	
P024	45	M	20	−	
P025	79	M	50	+	
P026	85	M	22	+	
P027	52	M	30	+	
P028	62	M	41	−	
P029	64	M	31	−	
P030	25	M	50	−	
P031	76	M	46	−	
P032	56	M	51	−	
P033	78	M	57	+	
P034	73	M	100	+	
P035	85	M	100	+	Figure 7
P036	89	M	75	+	
P037	72	M	25	+	
P038	56	M	48	+	
P039	60	M	20	+	
P040	65	M	27	+	
P041	80	M	48	−	
P042	53	M	95	+	
P043	53	M	100	+	
P044	75	M	100	+	
Average	66.8		51.2		
			Polarity distribution	N: 4.5%; Negative: 29.5%	
Total:	44		38% Females		

4. Conclusions

We presented a viable solution for the measurement of the WCT amplitude in a clinical setting. Our electrocardiographic device does not require the patient to be encased in a metallic structure submerged in water. Employing the latest components and printed circuit board technologies, we produced a compact design that employs standard ECG cables and electrode placement. Our ongoing clinical trial using this device has already confirmed the inadequateness of the WCT as a neutral reference for ECG signals. Our measurements performed on 44 volunteer patients confirmed that the WCT amplitude relative to lead II amplitude (average across the entire study's population), is 51.2% (standard deviation of 27.4%), with peaks of over 100%. Our measurements also confirmed, as

foreseen by Frank in the 1950s, that the WCT is another ECG lead with a high amplitude and typical characteristic waveforms, hence it should be included in the signal space used to diagnose diseases. We are currently assessing the clinical implications of our finding and continuing the data-recording campaign with the aim of collecting a larger, statistically significant sample of recordings, which will be released to researchers upon request.

Acknowledgments: The authors wish to thank the patients at Campbelltown Hospital (NSW) who volunteered for this study, and the nurses and the ECG technicians who helped with the data collection. The authors also gratefully acknowledge Texas Instruments who supplied chip samples for the construction of the prototype. This study is funded by the office for Research Engagement and Development with Industry (REDI) at the Western Sydney University and by the MARCS Institute (Biomedical Engineering and Neuro-Science BENS group).

Author Contributions: G.D.G. invented the technology, designed the hardware and conceived the study, M.C. and P.B. contributed to the design of the hardware, A.L.M., J.C.T. and H.M. contributed to the measurement analysis and data collection; I.M.S., A.O.L. and A.T. contributed to the design of the clinical study and facilitated the recording in hospital.

Conflicts of Interest: The authors declare no competing interests.

Appendix A

Reconstruction of cardinal leads from limb components

As mentioned in the methods section, device bandwidth and gains have been verified using a proper signal generator, capable of generating 1 mV_{pp} sine waves (Medi Cal Instruments model 220 Biomedical Function Generator) [26]. In addition, we assessed the point to point correlation between limb leads reconstructed using the limb components and limb leads that are recorded directly. To reconstruct the limbs, we simply operated a point by point subtraction between recorded signals and assessed the correlation between signals using the embedded MATLAB correlation function [19,20].

As an example (see Figure A1) we can compute lead I from simple subtraction of the WCT's components Left Arm(LA) and Right Arm (RA) (lead I = LA − RA [1]). In all the assessed cases, correlation scored in excess of 99% and signals cannot be distinguished unless labeled and plotted on different axis. We conclude that the LA, RA and LL components that we record with our device are the actual components of the WCT.

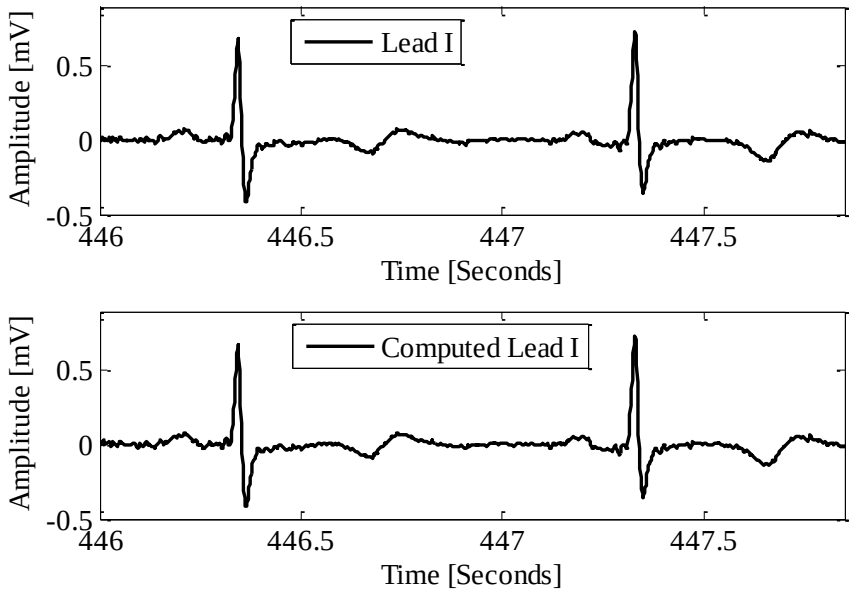

Figure A1. Example reconstruction of limb leads from components (P016). In this example, we reconstructed (computed) lead I from the LA and RA potentials recorded by our hardware; correlation between signals scored in excess of 99%.

References

1. Malmivuo, J.; Plonsey, R. *Bioelectromagnetism: Principles and Applications of Bioelectric and Biomagnetic Fields*; Oxford University Press: Oxford, UK, 1995.
2. Frank, E. General theory of heart-vector projection. *Circ. Res.* **1954**, *2*, 258–270. [CrossRef] [PubMed]
3. Bayley, R.H.; Reynolds, E.W.; Kinard, C.L.; Head, J.F. The Zero of Potential of the Electric Field Produced by the Heart Beat: The Problem with Reference to Homogeneous Volume Conductors. *Circ. Res.* **1954**, *2*, 4–13. [CrossRef] [PubMed]
4. Bayley, R.H.; Kinard, C.L. The Zero of Potential of the Electric Field Produced by the Heart Beat: The Problem with Reference to living human subject. *Circ. Res.* **1954**, *2*, 104–111. [CrossRef] [PubMed]
5. Horowitz, P.; Hill, W.; Robinson, I. *The Art of Electronics*; Cambridge University Press: Cambridge, UK, 1980.
6. Sedra, A.S.; Smith, K.C. *Microelectronic Circuits*; Oxford University Press: Oxford, UK, 2004.
7. Northrop, R.B. *Analysis and Application of Analog Electronic Circuits to Biomedical Instrumentation*; CRC Press: Boca Raton, FL, USA, 2012.
8. Webster, J. *Medical Instrumentation: Application and Design*; John Wiley & Sons: Hoboken, NJ, USA, 2009.
9. Enderle, J.D. *Bioinstrumentation*; Morgan & Claypool: Williston, VT, USA, 2006.
10. Gargiulo, G.; Bifulco, P.; Calvo, R.A.; Cesarelli, M.; Mcewan, A.; Jin, C.; Ruffo, M.; Romano, M.; Shephard, R.; Schaik, A.V. Giga-ohm high-impedance fet input amplifiers for dry electrode biosensor circuits and systems integrated microsystems: Electronics, photonics, and biotechnology ed k iniewski. In *Integrated Microsystems: Electronics, Photonics, and Biotechnology*; CRC Press: Boca Raton, FL, USA, 2011.
11. Bronzino, J.D. *Biomedical Engineering Handbook*; CRC Press: Boca Raton, FL, USA, 1999.
12. Burger, H.; Van Milaan, J. Heart-vector and leads: Part III geometrical representation. *Br. Heart J.* **1948**, *10*, 229–233. [CrossRef]
13. Burger, H.; Van Milaan, J. Heart-vector and leads. Part II. *Br. Heart J.* **1947**, *9*, 154–160. [CrossRef] [PubMed]
14. Wilson, F.N.; Johnston, F.D.; Rosenbaum, F.F.; Barker, P.S. On einthoven's triangle, the theory of unipolar electrocardiographic leads, and the interpretation of the precordial electrocardiogram. *Am. Heart J.* **1946**, *32*, 277–310. [CrossRef]
15. Burger, H.C.; Van Milaan, J. Heart-vector and leads. *Br. Heart J.* **1946**, *8*, 157–161. [CrossRef] [PubMed]
16. INA116—Texas Instruments. Available online: http://www.ti.com/lit/ds/symlink/ina116.pdf (accessed on 1 May 2016).
17. Gargiulo, G.D.; Tapson, J.; van Schaik, A.; McEwan, A.; Thiagalingam, A. Unipolar ecg circuits: Towards more precise cardiac event identification. In Proceedings of the 2013 IEEE International Symposium on Circuits and Systems (ISCAS2013), Beijing, China, 19–23 May 2013; pp. 662–665.
18. Gargiulo, G.; Thiagalingam, A.; Mcewan, A.; Cesarelli, M.; Bifulco, P.; Tapson, J.; van Schaik, A. True unipolar ecg leads recording (without the use of wct). *Heart Lung Circ.* **2013**, *22*, S102. [CrossRef]
19. Gargiulo, G.D.; Varaki, E.S.; Hamilton, T.J.; Bifulco, P.; Cesarelli, M.; Romano, M. A 9-independent-leads ecg system from 10 electrodes: A practice preserving wct-less true unipolar ecg system. In Proceedings of the Biomedical Circuits and Systems Conference (BioCAS), Atlanta, GA, USA, 22–24 October 2015; pp. 1–4.
20. Gargiulo, G.D. True unipolar ecg machine for wilson central terminal measurements. *BioMed. Res. Int.* **2015**, *2015*, 586397. [CrossRef] [PubMed]
21. Gargiulo, G.; McEwan, A.; van Schaik, A.; Jin, C.; Cesarelli, M.; Bifulco, P.; Calvo, R.A. *Non-Invasive Electronic Biosensor Circuits and Systems*; INTECH Open Access Publisher: Rijeka, Croatia, 2010.
22. Prance, R.J.; Beardsmore-Rust, S.; Aydin, A.; Harland, C.J.; Prance, H. Biological and medical applications of a new electric field sensor. In Proceedings of the ESA Annual Meeting in Electrostatics, Minneapolis, MN, USA, 17–19 June 2008; pp. 1–4.
23. Prance, R.J.; Debray, A.; Clark, T.D.; Prance, H.; Nock, M.; Harland, C.J.; Clippingdale, A.J. An ultra-low-noise electrical-potential probe for human-body scanning. *Meas. Sci. Technol.* **2000**, *11*, 291–297. [CrossRef]
24. CG/CG2 SN Series—Medium to High Surge GDT from Gas Discharge Tubes. Available online: http://www.littelfuse.com/products/gas-discharge-tubes/medium-to-high-surge-gdt/cg-cg2-sn.aspx (accessed on 1 May 2016).
25. OPA140 High-Precision, Low-Noise, Rail-to-Rail Output, 11-MHz JFET Op Amp. Available online: http://www.ti.com/lit/ds/symlink/opa4140.pdf (accessed on 1 May 2016).

26. Gargiulo, G.D.; Bifulco, P.; Cesarelli, M.; Fratini, A.; Romano, M. Problems in assessment of novel biopotential front-end with dry electrode: A brief review. *Machines* **2014**, *2*, 87–98. [CrossRef]
27. Gargiulo, G.D.; McEwan, A.L.; Bifulco, P.; Cesarelli, M.; Jin, C.; Tapson, J.; Thiagalingam, A.; van Schaik, A. Towards true unipolar bio-potential recording: A preliminary result for ecg. *Physiol. Meas.* **2012**, *34*, N1. [CrossRef] [PubMed]
28. Winter, B.B.; Webster, J.G. Reduction of interference due to common mode voltage in biopotential amplifiers. *IEEE Trans. Biomed. Eng.* **1983**, *30*, 58–62. [CrossRef] [PubMed]
29. Gargiulo, G.; McEwan, A.; Bifulco, P.; Cesarelli, M.; Jin, C.; Tapson, J.; Thiagalingam, A.; Van Schaik, A. Towards true unipolar ecg recording without the wilson central terminal (preliminary results). *Physiol. Meas.* **2013**, *34*, 991–1012. [CrossRef] [PubMed]
30. Akay, M. *Wiley Encyclopedia of Biomedical Engineering*; John Wiley & Sons: Hoboken, NJ, USA, 2006.
31. Hwang, I.-D.; Webster, J.G. Direct interference canceling for two-electrode biopotential amplifier. *IEEE Trans. Biomed. Eng.* **2008**, *55*, 2620–2627. [CrossRef] [PubMed]
32. Gargiulo, G.D.; Bifulco, P.; Cesarelli, M.; McEwan, A.; Wabnitz, A. Open platform, 32-channel, portable, data-logger with 32 PGA control lines for wearable medical device development. *Electron. Lett.* **2014**, *50*, 1127–1129. [CrossRef]